JOURNAL OF CATALYSIS **176,** 143–154 (1998)
ARTICLE NO. CA982056

Selective Oxidation of 1-Butene over Silica-Supported Cr(VI), Mo(VI), and W(VI) Oxides

Narayanan C. Ramani,* David L. Sullivan,* John G. Ekerdt,*,[1] Jih-Mirn Jehng,†,[2] and Israel E. Wachs†

*Department of Chemical Engineering, The University of Texas at Austin, Austin, Texas 78712; and †Zettlemoyer Center for Surface Studies and Department of Chemical Engineering, Lehigh University, Bethlehem, Pennsylvania 18015

Received September 4, 1997; revised February 18, 1998; accepted February 23, 1998

The role of surface structure and cation red-ox nature was investigated for the selective oxidation of 1-butene over SiO_2-supported Mo(VI), Cr(VI), and W(VI) oxide catalysts. X-ray diffraction and Raman spectroscopy were used to characterize the surface structures over the different catalysts. The surface structure of Mo(VI)/SiO_2 was controlled by using different preparation methods. An aqueous route using $(NH_4)_6Mo_7O_{24}$ led to a catalyst that had dispersed Mo along with small crystallites of MoO_3. Organometallic routes using $(C_5H_5)_2Mo_2(CO)_6$ and $Mo(C_3H_5)_4$ led to completely dispersed Mo(VI)/SiO_2. $Cr(NO_3)_3$ was used to prepare completely dispersed Cr(VI)/SiO_2. In the case of W(VI)/SiO_2, the dispersion depended on the type of SiO_2 employed. The activity to formation of 1,3-butadiene revealed a structure effect for the Mo(VI)/SiO_2 catalysts, with crystalline Mo(VI) having a higher activity than dispersed Mo(VI). The red-ox ability of the supported cation was seen to have a dominating effect for this reaction. The turnover number for the formation of 1,3-butadiene followed the order Cr(VI)/SiO_2 > Mo(VI)/SiO_2 ≫ W(VI)/SiO_2, which is in agreement with the red-ox ability Cr > Mo > W. The importance of red-ox ability is discussed in terms of the allylic abstraction mechanism that is involved in selective oxidation.

INTRODUCTION

Selective oxidation reactions are involved in a wide variety of applications including the production of synthetic rubber, fine chemicals, and plastics, and even in pollution control. Numerous studies have been carried out in this area, and some of the more recent review articles provide a good background (1–5). Most selective oxidation reactions involve hydrocarbons and O_2 in the feed, resulting in a very complex network of competing reactions. Breaking a C–H bond is one of the basic steps in all these selective oxidation reactions. In some cases oxygen is incorporated into the hydrocarbon; in others, it combines with the abstracted hydrogen atoms to form water. Bulk oxides, or mixed metal oxides, with a host of promoters have been the preferred industrial catalysts for these reactions (6). The presence of different promoters makes it hard to separate out the role played by different cations, and thus complicates understanding the basic steps involved in selective oxidation.

In recent years there has been an effort to study selective oxidation over well characterized supported metal oxides without promoters (7–9). This has been partly fueled by the fact that a variety of spectroscopic characterization techniques including Raman spectroscopy, extended X-ray absorption fine structure spectroscopy, solid state nuclear magnetic resonance, and X-ray absorption near edge spectroscopy have led to a very good understanding of supported metal oxide surfaces. Important issues in selective oxidation reactions like structure sensitivity (isolated cations or crystallites), oxygen ligand type (M=O [oxo] or M–O–Si [bridging]; M = supported cation, i.e. Cr, Mo, or W), the red-ox nature of the cation, and the nature of the acid sites on the catalyst surface can be studied in greater detail, as these supported metal oxide systems provide the ideal template to do so.

Structure sensitivity has been previously explored for a number of reactions and systems (10, 11). Ono *et al.* and other groups have shown that dispersed, surface polymolybdates have a much higher activity for ethanol oxidation than bulk MoO_3 (12, 13). Similar results have been obtained for methanol oxidation over supported V, Cr, and Mo oxides (14–16). In some studies, the activity in selective oxidation reactions has been attributed to the strength of the M=O bond, while others have emphasized the role of the support through the bridging M–O–Si bond (17–20). Deo *et al.* have reported that the turnover frequency for methanol oxidation varies by three orders of magnitude when going from V/TiO_2 to V/SiO_2, although *in situ* Raman spectroscopy revealed that the extent of cation reduction was the same (9). They suggest that even though the number of active sites was comparable, the activity per site was very different and was affected by the M–O-support ligand. Zhang *et al.* have looked at ethanol oxidation over

[1] Corresponding author. E-mail: ekerdt@che.utexas.edu.
[2] Current address: Department of Chemical Engineering, National Chung-Hsing University, Taichung 402, Taiwan.

0021-9517/98 $25.00

supported Mo and obtained similar results (13). They attributed the two orders of magnitude difference in activity of Mo/TiO_2 versus Mo/SiO_2 to the differences in the electronic partition function associated with the density of electron accepting states in the molybdate-support complex. The density of available states has been observed to correlate with the red-ox ability of the surface oxide–support complex (21). This link to the red-ox ability of the catalyst is in agreement with the theoretical calculations of Weber for methanol oxidation over supported Mo oxides (22).

While these attempts to unravel the role of structure sensitivity and the red-ox nature of these supported metal oxides has shed some light on the controlling factors responsible for selective oxidation, the bulk of the work has concentrated on alcohol oxidation and simple molecules like methanol. It is of great interest to see how these ideas can be explored for more complex reaction systems like 1-butene oxidation. Alkenes can undergo isomerization, dehydrogenation with and without oxygen insertion into the parent hydrocarbon, and nonselective oxidation to CO and CO_2. The reaction network of 1-butene oxidation is shown in Fig. 1. Isomerization of 1-butene to 2-butenes is a side reaction that can proceed through a Bronsted catalyzed pathway or an allylic pathway, as discussed in detail previously (23). Selective oxidation takes place through the allylic route, where the first step involves hydrogen abstraction. Subsequently, the allyl on the surface can undergo another hydrogen abstraction step to yield the desired product, 1,3-butadiene. Oxygen insertion into the allyl is also possible, and this could lead to the formation of oxygenated products like crotonaldehyde or methyl vinyl ketone. Such products have been observed by Escribano *et al.* in infrared spectroscopy studies of butene adsorption over supported V systems (24). The oxygenated products are strongly adsorbed on the catalyst surface and this can lead to nonselective oxidation of 1-butene to CO and CO_2.

Much of the past 1-butene oxidation work has concentrated on bulk and mixed metal oxides (6, 11). Very few studies can be found where the reaction of 1-butene has been studied over supported metal oxides. Mori *et al.* reported that the activity in the selective oxidation of 1-butene over V_2O_5/TiO_2 and V_2O_5/Al_2O_3 was controlled by the number of V=O species on the catalyst (25). They also attributed the higher activity of the V_2O_5/TiO_2 compared to the V_2O_5/Al_2O_3 catalysts to a structure effect, but no details were provided. Kung and Kung found that in the selective oxidation of 1-butene over bulk α-Fe_2O_3 and supported α-Fe_2O_3/SiO_2, the activity did not vary much, but the selectivity varied with crystallite size (11). Structure effects in terms of completely dispersed cations versus crystallites have not been explored before for 1-butene oxidation. Also, to understand the role of red-ox nature, a more comprehensive study involving different supported cations and supports is required.

For exploring the 1-butene reaction network over supported metal oxides, we have chosen the SiO_2-supported metal oxides of Cr(VI), Mo(VI), and W(VI) as model templates for a number of reasons. The three supported cations selected are ideal to explore cation red-ox nature, as they belong to group VIB in the periodic table with decreasing red-ox nature. Other important factors are that the surface structures of these cations on SiO_2 are well understood and that SiO_2 is a relatively inert support (26–31). In the case of the $Mo(VI)/SiO_2$ system, control of the type of surface structure is also possible by employing different preparation methods, and thus structure sensitivity of the 1-butene reaction can be explored. If aqueous routes are followed, crystallites of MoO_3 are present, along with

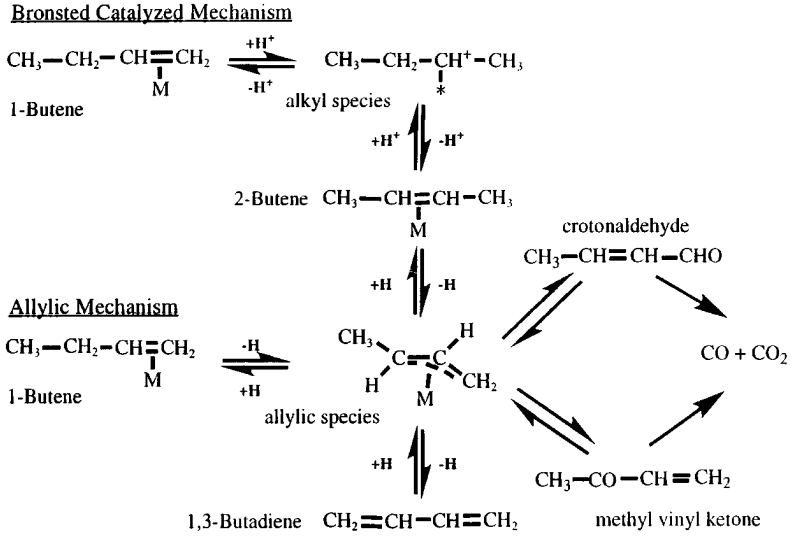

FIG. 1. Reaction pathways for 1-butene oxidation.

dispersed Mo species, even at very low weight loadings (0.4%) (29). We have previously shown that organometallic preparation methods can lead to completely dispersed Mo species up to 6.4% Mo on SiO_2 (Davison 952) before crystallites of MoO_3 are observed (29, 32). This weight loading corresponds to the point where all the SiO_2 hydroxyl groups have reacted with the organometallic precursor. The dehydrated, dispersed Mo(VI) species has MoO_5 coordination, with one oxo (Mo=O) and four bridging oxygen ligands (Mo–O–Si). Similar results were obtained for the $W(VI)/SiO_2$ (Davison 952) system (30, 31).

For the $Cr(VI)/SiO_2$ system, an isolated dispersed species is present up to 2% Cr. Initially, Wachs and co-workers assigned a tetrahedral di-oxo structure to the Cr cation, but more recent work by that group involving ^{16}O–^{18}O isotope experiments has suggested that the Cr cation on different oxide supports has only one oxo ligand (33). In an X-ray photoelectron spectroscopy (XPS) study, Merryfield *et al.* have conclusively shown that completely oxidized 1.1 wt% Cr/SiO_2 contained only Cr(VI) based on the single Cr $2p_{3/2}$ peak at 581.6 eV (34). The corresponding Cr $2p_{3/2}$ peaks for Cr(IV) and Cr(II) were found at 577.6 and 576.6 eV for other samples. Kim and Woo used temperature-programmed oxidation/temperature-programmed reduction (TPO/TPR) and infrared spectroscopy (IR) to study 1.1 wt% Cr/SiO_2 and concluded that the average oxidation state of the surface Cr was between 6.0 and 5.4 for activation temperatures up to 823 K (35). A number of diffuse reflectance spectroscopy (DRS) studies have shown that for low weight loading Cr/SiO_2, the Cr species is initially present as Cr(VI) before undergoing reduction during polymerization reactions (36–38). Recent UV-Vis DRS data of Weckhuysen *et al.* suggest that all the Cr on SiO_2 at low weight loadings is present as a dispersed species and they find no evidence for crystalline Cr_2O_3 (39). Thus, the picture that emerges is that at low weight loadings (<2 wt% Cr) Cr is predominantly isolated, dispersed, and in a 6+ oxidation state. At higher loadings, both dispersed Cr species (Cr(VI), Cr(III)) and crystallites of Cr_2O_3 are present (40).

The similarity in surface structures of the dispersed Cr, Mo, and W cations provides a means to explore red-ox ability for 1-butene oxidation.

METHODS

Two methods were used to prepare the supported Mo(VI) oxides on SiO_2 (Cab-O-Sil HS 5 [Cabot]; 325 m^2/g). In the first method, organometallic routes were followed using $(C_5H_5)_2Mo_2(CO)_6$ or $Mo(C_3H_5)_4$. A more complete description of these routes can be found elsewhere (41, 42). After attaching the precursors to the surface through the SiO_2 hydroxyl groups, a temperature ramp in flowing He results in desorption of the remaining ligands. The samples were then calcined in hydrocarbon free air (HFA) at 773 K for 8 h. An aqueous route using $(NH_4)_6Mo_7O_{24}$ was followed in the second method. The samples made by this method were first dried at 423 K for 5 h before being calcined at 773 K in HFA for 8 h. To investigate the role of the SiO_2 support in dispersing W, three different commercially available SiO_2 samples were utilized (Cab-O-Sil HS 5, Davison 952 [W.R. Grace; 300 m^2/g], and Silice X400LS [Rhone Poulenc; 325 m^2/g]). Organometallic routes using $(C_5H_5)_2W_2(CO)_6$ or $W(C_3H_5)_4$ were followed for making the supported W(VI) oxide catalysts; the Mo heating schedule was followed. The $Cr(VI)/SiO_2$ (Cab-O-Sil HS 5) catalysts were prepared by an aqueous method using $Cr(NO_3)_3$. These samples were dried at 423 K for 5 h before being calcined at 773 K in HFA for 8 h.

The weight loadings for Mo (1.7 to 8.4%) and Cr (0.1 to 3.8%) were obtained by atomic absorption spectroscopy (AAS); the weight loadings for W (2.7 to 5.6%) were determined by Galbraith Laboratories. The accuracy of the AAS measurement for Cr in the 0.1% $Cr(VI)/SiO_2$ sample was estimated to be ±15%. The surface areas of the catalysts were measured by N_2 BET and found not to vary appreciably from that for the blank SiO_2. The surface structures of the catalysts were characterized by X-ray diffraction (XRD) and Raman spectroscopy. Powder XRD was performed on a Phillips PW 1729 X-ray generator using Cu Kα radiation ($\lambda = 1.54$ Å) at 40 kV and 40 mA. The data collection time was 12 s per step (0.05°), in order to increase the signal to noise ratio so that even very small peaks could be observed and resolved. Both *in situ* and ambient Raman spectroscopy were carried out at Lehigh University on a Spex Triplemate spectrometer using an Ar^+ ion laser delivering about 40 mW of power. All samples were calcined at 773 K overnight before being pressed into wafers for Raman spectroscopy. Raman procedures are described elsewhere (20). Despite the pretreatment, many of the samples, especially the $Cr(VI)/SiO_2$ catalysts exhibited strong fluorescence.

The flow reactor experiments were carried out in a 0.5 mm ID quartz u-tube reactor. The amount of catalyst used varied between 50 and 100 mg. The samples were initially calcined at 773 K in HFA, before being cooled to the reaction temperature in HFA. A 5000 ppm mixture of 1-butene in He and a 2% O_2 in He mixture were used. The flows were such that a 1:1 molar ratio of 1-butene to O_2 was present. The total flow rate varied between 25 and 100 standard cubic centimeters per minute (sccm). The variation in catalyst weight and total flow rate was such that conversion of 1-butene to oxidation products was between 1 and 20%. Conversions were calculated assuming that both 1-butene and 2-butenes were reactant species. The system was allowed to reach steady state (typically 1 h) before data were obtained. The temperature was sequentially increased to the next value. For some samples, activity

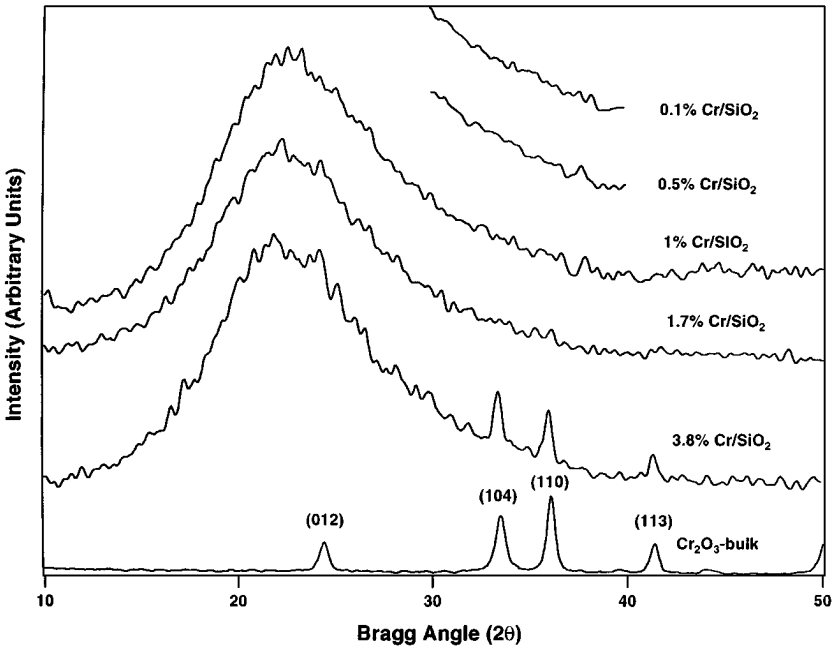

FIG. 2. X-ray diffraction patterns of $Cr(VI)/SiO_2$ catalysts.

data were collected while both sequentially increasing and decreasing the temperature in order to ensure that there were no hysteresis effects. The data agreed to within ±5%. The effluent from the reactor was sampled on-line with a Hewlett-Packard 5880A gas chromatograph equipped with a flame ionization detector and a thermal conductivity detector. An SP 1700 column was used to separate the hydrocarbons, and a combination of 5 Å molecular sieve and PoraPLOT Q columns was used to detect CO and CO_2. Certified gas mixtures from Matheson and Liquid Carbonic Industries were used to calibrate detector sensitivities and retention times for reactants and products.

RESULTS

Figures 2, 3, and 4 show the XRD patterns of a series of $Cr(VI)/SiO_2$, $Mo(VI)/SiO_2$, and $W(VI)/SiO_2$ catalysts (on Cab-O-Sil HS 5), respectively. The XRD pattern of

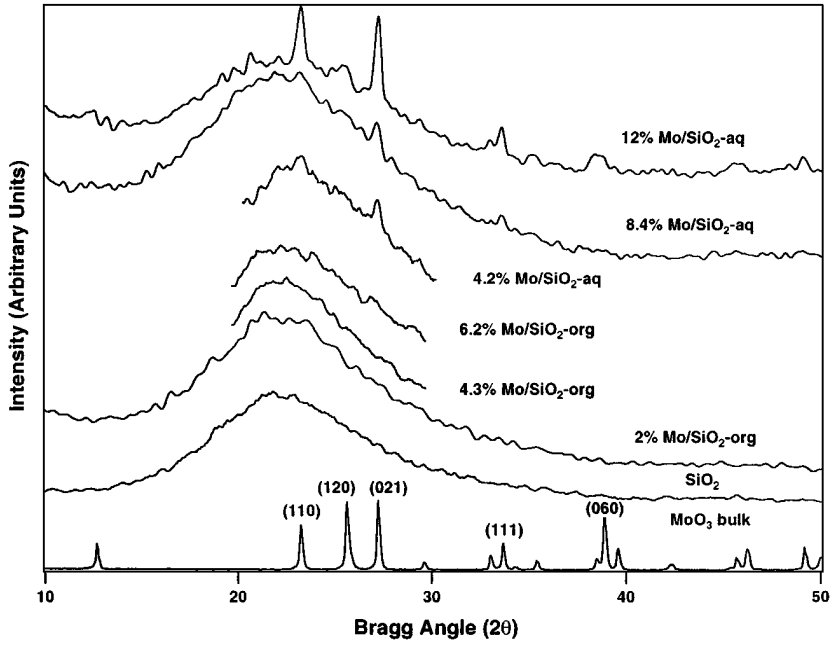

FIG. 3. X-ray diffraction patterns of $Mo(VI)/SiO_2$ catalysts.

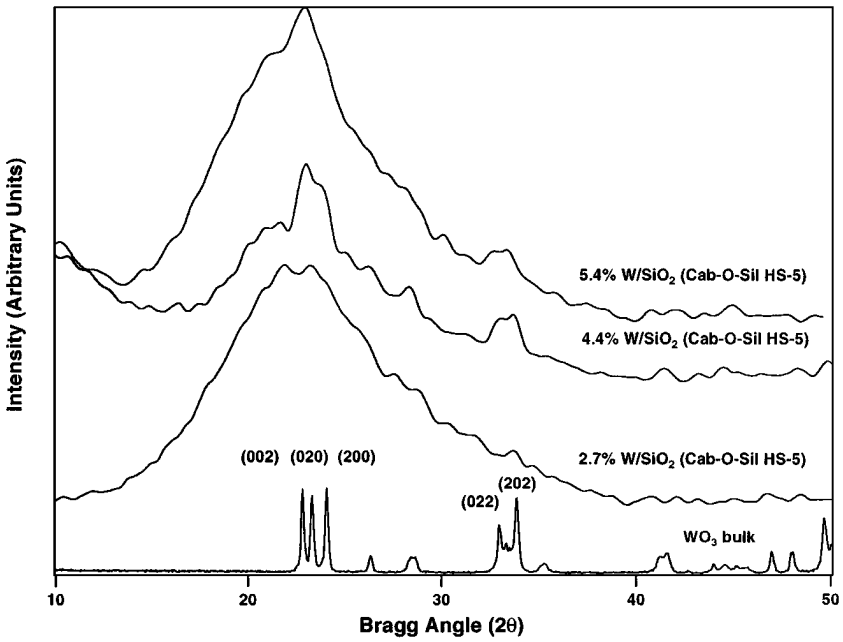

FIG. 4. X-ray diffraction patterns of W(VI)/SiO_2 (Cab-O-Sil HS 5) catalysts.

Cab-O-Sil HS 5 SiO_2 is also shown in Fig. 3 for comparison. The XRD patterns of the bulk oxides (Cr_2O_3, MoO_3, and WO_3) are shown at the bottom of the respective figures. The broad feature in all the patterns arises from the amorphous SiO_2. Over the low weight loading Cr(VI)/SiO_2 catalysts (0.1 to 1.0% Cr), no features attributable to crystalline Cr_2O_3 can be seen. In the 3.8% Cr(VI)/SiO_2 sample, the (104), (110), and (113) peaks of crystalline Cr_2O_3 can be clearly observed. In the case of the Mo(VI)/SiO_2 catalysts (Fig. 3), the (110) and (021) peaks of crystalline MoO_3 can be seen for the samples made via the aqueous route at weight loadings of 4.2 to 12%. For the samples made via the organometallic route (2.0 to 6.2%), no peaks from crystalline MoO_3 can be observed. Over W(VI)/SiO_2 (Cab-O-Sil HS 5) catalysts, some crystalline WO_3 can be observed over the higher weight loading catalysts, even though organometallic preparation methods were used in an effort to avoid crystallites.

Figure 5 shows the Raman spectra of the 1.0% Cr(VI)/SiO_2 sample under both ambient and dehydrated, *in situ* conditions. Under ambient conditions, broad features are observed at 986, 895, and 450 cm^{-1}. The broad feature centered at 450 cm^{-1} arises from the SiO_2 support. The 895 cm^{-1} band has been previously assigned to the asymmetric and symmetric CrO_3 stretches of the CrO_4^{2-} and $Cr_2O_7^{2-}$ species on the surface (43). The 986 cm^{-1} band has been assigned to the symmetric Cr=O stretch of a dehydrated, isolated Cr species; the local dehydration due to the laser interacting with the sample (15, 40, 43). For the dehydrated, *in situ* Raman spectra of the 1.0% Cr(VI)/SiO_2 catalyst, an intense background is observed due to fluorescence. Despite the fluorescence, a feature at 986 cm^{-1} that arises from a dehydrated, isolated Cr species is observed (15, 40). No Raman features of crystalline Cr_2O_3 (600 and 543 cm^{-1}) are observed. The Raman spectra of the other Cr samples could not be obtained due to fluorescence.

The dehydrated, *in situ* Raman spectra of selected Mo(VI)/SiO_2 catalysts made via both the aqueous and organometallic routes are presented in Fig. 6. The Mo(VI)/SiO_2 catalysts made via the organometallic route (2.0 and 6.2% Mo) have similar Raman spectra, with an intense peak at 993 cm^{-1} from an isolated Mo species and broad features at 820, 610, and 450 cm^{-1} arising from the SiO_2 support (27, 29, 44). For the Mo(VI)/SiO_2 samples made via the aqueous route (4.2 and 8.4% Mo), the intense feature at 816 cm^{-1} from the Mo–O stretching mode of crystalline MoO_3 dominates the spectrum (16, 29). Williams *et al.* also observed crystallites of MoO_3, even at 0.4% Mo, when aqueous routes were used to make Mo(VI)/SiO_2 catalysts (29).

Previous work had shown that it is possible to disperse up to 9.6% W on Davison SiO_2 using organometallic preparation methods (30); the XRD patterns of 5.4% W(VI)/SiO_2 (Cab-O-Sil HS 5) (Fig. 4) suggest the presence of crystalline WO_3 for samples made following the same preparation methods. To investigate the role of the SiO_2 support, W dispersion by organometallic routes was studied over three different commercial silicas. The Raman spectra of W supported on the three SiO_2 supports are presented in Fig. 7. For the catalysts made using Silice and Davison SiO_2, the Raman spectra show a small peak at 990 cm^{-1}, consistent with an isolated W cation (30, 31). Other features at ~800 and ~600 cm^{-1} and the broad feature between

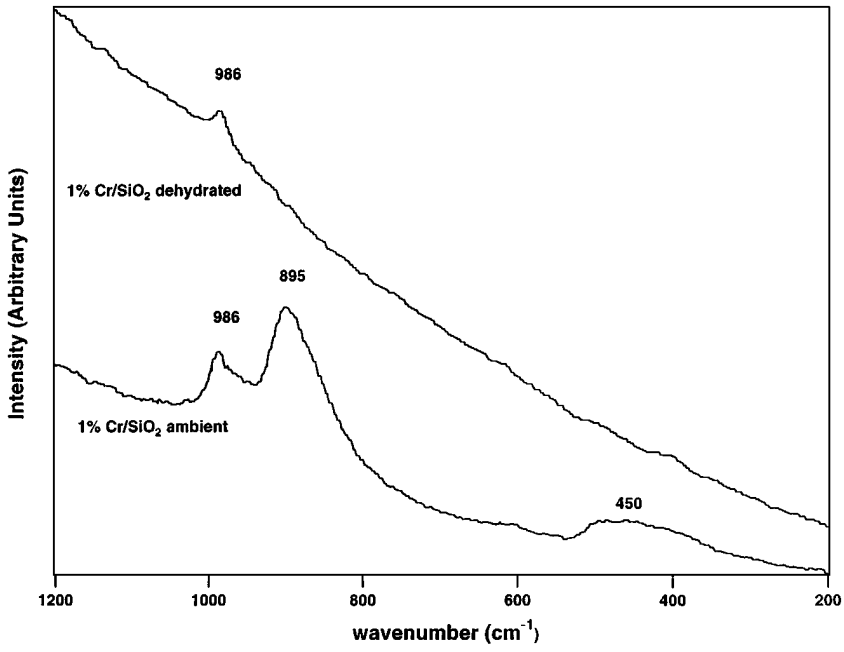

FIG. 5. Raman spectra of 1.0% Cr(VI)/SiO_2 catalyst.

485 and 300 cm^{-1} are characteristic Raman features of the SiO_2 support. In the case of the Cab-O-Sil HS 5 supported W(VI)/SiO_2, intense features at 810 and 720 cm^{-1} can be observed. These have been previously assigned to W–O stretching modes of crystalline WO_3 (30, 31). Thus, dispersion of W is not the same on the different SiO_2 supports and could be due to the texture of the SiO_2 support or the different impurities present in the supports (Table 1). Dispersion was not explored in detail since all the W catalysts had very low oxidation activities at the conditions employed herein.

Figures 8, 9, and 10 show the activity to butadiene formation based on catalyst BET area (moles/m^2-s) for a series of W(VI)/SiO_2 (Cab-O-Sil HS 5), Mo(VI)/SiO_2, and Cr(VI)/SiO_2 catalysts, respectively. The main products of the reaction of 1-butene were 2-butenes, 1,3-butadiene, CO, and CO_2. The blank activity over the SiO_2 support

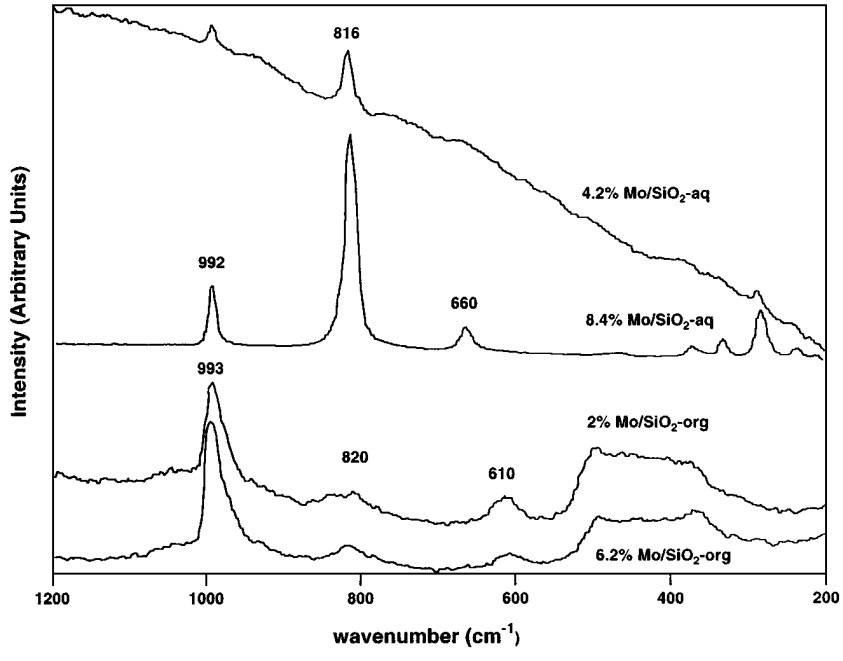

FIG. 6. Raman spectra of Mo(VI)/SiO_2 catalysts.

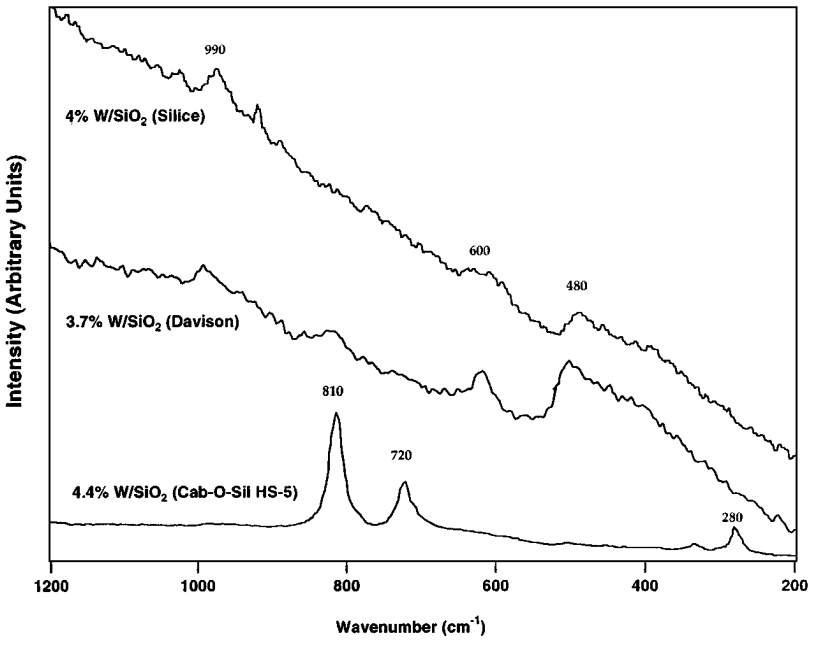

FIG. 7. Raman spectra of W(VI)/SiO_2 catalysts supported on different SiO_2 supports.

is also shown in these figures for comparison. For all the W(VI)/SiO_2 catalysts, the activity to butadiene formation is very low and is similar to that of blank SiO_2. In previous work, 1-butene isomerization on W(VI)/SiO_2 was studied under identical conditions and we did not observe hysterisis in the rate of 1-butene isomerization from 300 to 773 K and back to 300 K (23). If the W(VI) centers had been deactivated at the higher temperatures due to coking, the rates of isomerization should have been markedly different when measured a second time. We also monitored 1,3-butadiene formation with respect to time and temperature and found no change in the activity or selectivity. Thus, the low activity

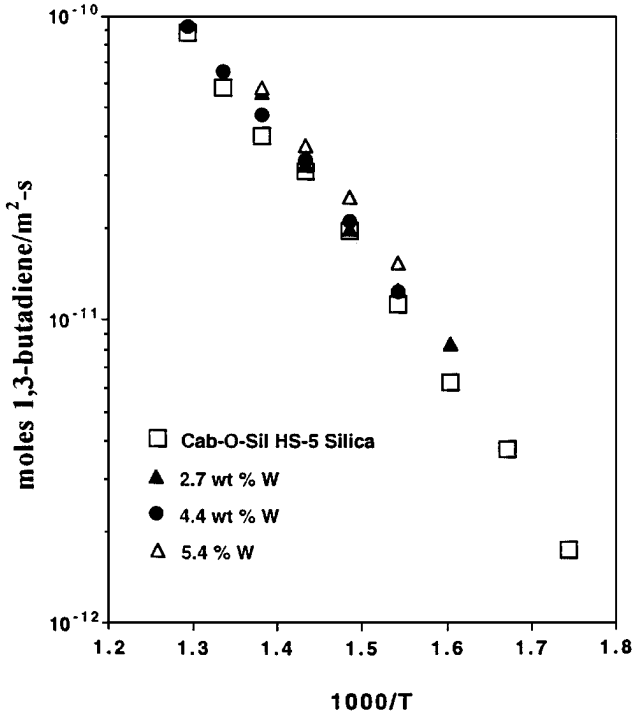

FIG. 8. Rate of formation of 1,3-butadiene over W(VI)/SiO_2 catalysts.

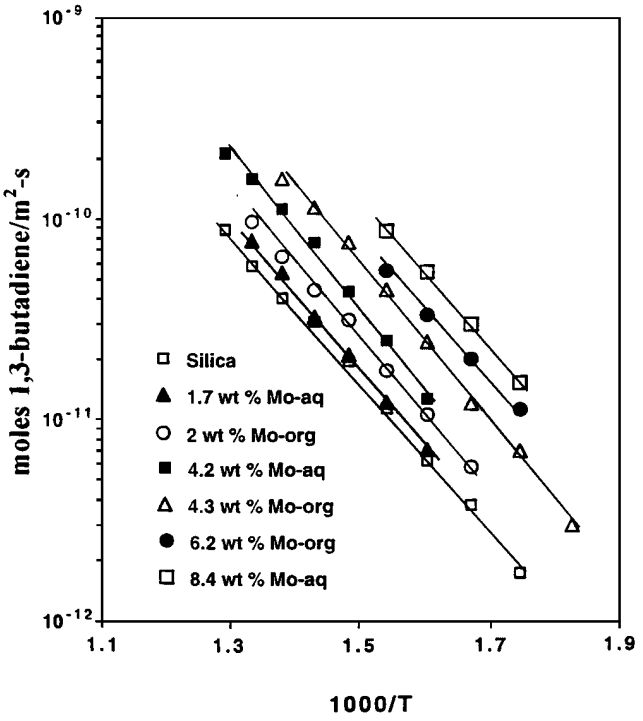

FIG. 9. Rate of formation of 1,3-butadiene over Mo(VI)/SiO_2 catalysts.

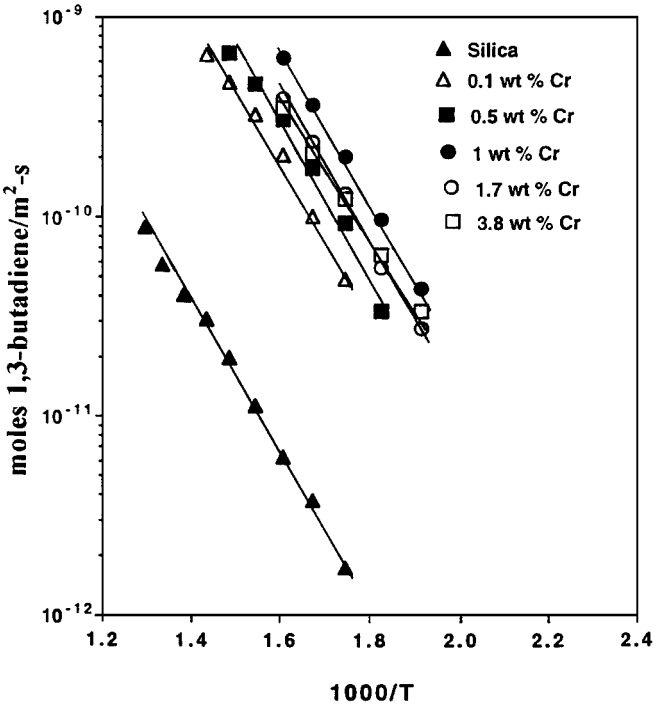

FIG. 10. Rate of formation of 1,3-butadiene over $Cr(VI)/SiO_2$ catalysts.

to 1,3-butadiene formation is the intrinsic activity of the $W(VI)/SiO_2$ catalysts and is not due to deactivation from coking. For $Mo(VI)/SiO_2$ catalysts, the activity is seen to increase with weight loading of Mo for both the catalysts made via the organometallic and the aqueous routes. The rate of formation of 1,3-butadiene for 8.4% $Mo(VI)/SiO_2$ is 10 times higher than that for the blank support. Compared to the $W(VI)/SiO_2$ or $Mo(VI)/SiO_2$ catalysts, the $Cr(VI)/SiO_2$ catalysts exhibit very high activities, even at low weight loadings. The activity of the 0.1% $Cr(VI)/SiO_2$ catalyst is three times higher than the 8.4% $Mo(VI)/SiO_2$ catalyst. The activity for butadiene formation also increases with weight loading from 0.1 to 1.0%, but it decreases slightly for the 1.7% and the 3.8% $Cr(VI)/SiO_2$ catalysts. Two percent is the approximate Cr loading at which Cr_2O_3 crystallites have been observed previously by Raman spectroscopy, and it is possible that the 1.7% $Cr(VI)/SiO_2$ sample has some Cr_2O_3 crystallites present (40). The 3.8% $Cr(VI)/SiO_2$ contains both dispersed Cr in the 6+ oxidation state and crystallites of Cr_2O_3, where the Cr is in the 3+ oxidation state.

The turnover frequencies (TOFs) at 623 K for $Mo(VI)/SiO_2$ catalysts made via the organometallic route are presented in Table 2. The TOFs were calculated assuming all the Mo is available in active sites. This is a very good assumption, as Raman spectroscopy has clearly established that Mo is completely dispersed on SiO_2 for catalysts made via organometallic routes. The TOF for bulk MoO_3 is also shown in Table 2 and is approximately three times higher than the TOF for supported $Mo(VI)/SiO_2$ catalysts made via the organometallic route. The TOF for bulk MoO_3 was calculated by assuming that one MoO_6 unit occupies 0.14 nm^2 and the number of Mo units available for reaction was determined by dividing the N_2 BET surface area by 0.14 nm^2 (45).

The presence of both dispersed Mo cations and crystallites of MoO_3 makes it difficult to accurately estimate TOFs for $Mo(VI)/SiO_2$ catalysts made via aqueous routes. In similar situations, Kim *et al.* have estimated the TOF on a total weight loading basis, although crystallites of MoO_3 were present along with dispersed Mo (16). Zhang *et al.* have used chemisorption techniques to estimate the number of active sites, although the number of dispersed sites versus the number of sites on crystallites could not be independently determined (13). In our case, calculating the apparent TOF on a nominal weight loading basis gives values of $0.14 \times 10^{-4}, 0.09 \times 10^{-4}$, and 0.21×10^{-4} for the 1.7, 4.2, and 8.4% $Mo(VI)/SiO_2$ catalysts made via the aqueous routes, respectively. The real TOFs for these catalysts are definitely higher than the estimated numbers, as the presence of crystallites of MoO_3 is shown by both XRD and Raman spectroscopy of these samples and implies that only some of the Mo cations are available for reaction.

The TOFs for the 0.1, 0.5, and 1.0% $Cr(VI)/SiO_2$ catalysts are compared at 623 K in Table 2. The TOFs for these catalysts were calculated assuming all the Cr was available in active sites for the reaction. Raman spectroscopy has established that completely dispersed Cr is present up to around 2% Cr (40). The TOFs for the low weight loading $Cr(VI)/SiO_2$ catalysts were at least 50 times higher than the dispersed $Mo(VI)/SiO_2$ catalysts. The TOF for bulk Cr_2O_3 is also included in Table 2, and it is 10 times lower than the dispersed $Cr(VI)/SiO_2$. One CrO_4 unit was assumed to occupy 0.21 nm^2 based on the crystal structure and the lattice parameters of α-Cr_2O_3 (46). For the 1.7 and 3.8% $Cr(VI)/SiO_2$, TOFs could not be accurately estimated as the presence of both a dispersed Cr phase and crystallites of Cr_2O_3 makes it difficult to calculate the number

TABLE 1

Impurity Content of the Different SiO_2 Supports[a]

Impurities	Cab-O-Sil HS 5 (ppm)	Davison (ppm)	Silice (ppm)
Aluminum	94	199	160
Calcium	16	150	81
Iron	14	48	98
Magnesium	47	44	83
Titanium	20	115	145
Zirconium	41	166	10

[a] Measured by Galbraith Laboratories, Knoxville, TN.

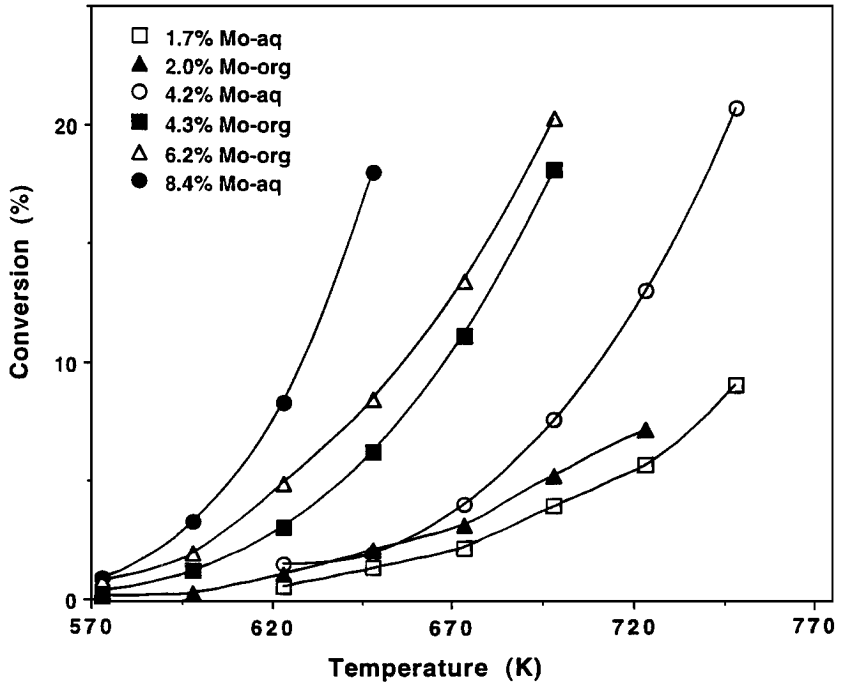

FIG. 11. Conversions over $Mo(VI)/SiO_2$ catalysts.

of sites available for reaction. If the nominal weight loadings are used, then the apparent TOFs for the 1.7 and 3.8% $Cr(VI)/SiO_2$ at 623 K are 4.0×10^{-4} and 1.6×10^{-4}, respectively. The real TOFs for these catalysts are somewhere in between that for the dispersed Cr and the bulk Cr_2O_3. The TOFs have not been reported for the $W(VI)/SiO_2$ catalysts, as no significant activity is seen over these catalysts when compared to the support.

The activation energies for these samples, as calculated from the Arrhenius plots, are presented in Table 2. Over all catalysts, the activation energies calculated were around 30 kJ/mol, except Cr_2O_3 which had an activation energy of 24.8 kJ/mol. Typical conversion data for the series of $Mo(VI)/SiO_2$ and $Cr(VI)/SiO_2$ catalysts are presented in Figs. 11 and 12. Conversions were calculated assuming that the 2-butenes were also reactants in the selective oxidation reaction. The conversions in all cases are below 20%, and are higher on the higher weight loading catalysts, as expected. The selectivity (at comparable conversions (5 to 8%)) to butadiene is between 35 and 40% for all the $Mo(VI)/SiO_2$ catalysts except for the 8.4% $Mo(VI)/SiO_2$ catalyst, which has a selectivity of 30%. The selectivity to butadiene is about 30% on the 0.1, 0.5, and 1.0% $Cr(VI)/SiO_2$ catalysts and is about 20% on the 1.7 and 3.8% $Cr(VI)/SiO_2$ catalysts. The low selectivity to 1,3-butadiene observed over the $Mo(VI)/SiO_2$ and $Cr(VI)/SiO_2$ catalysts reflects on the extent of reaction of 1-butene. Previous infrared spectroscopy work on the adsorption of 1-butene over these catalysts showed that the $Cr(VI)/SiO_2$ catalysts easily facilitate hydrogen abstraction from the allylic carbon and oxygen insertion into the hydrocarbon (24). Such oxygen insertion leads to the formation of crotonaldehyde or methyl vinyl ketone that strongly adsorb on the surface, and this may lead to non-selective oxidation to CO and CO_2.

TABLE 2

TOF and Activation Energies for 1-Butene Oxidation

Catalyst	TOF ($\times 10^4$) 1,3-butadiene (s^{-1})	Activation energy (kJ/mol)
0.1% $Cr(VI)/SiO_2$	21.0	30.0
0.5% $Cr(VI)/SiO_2$	9.6	31.1
1.0% $Cr(VI)/SiO_2$	11.1	31.1
1.7% $Cr(VI)/SiO_2$	[a]	31.9
3.7% $Cr(VI)/SiO_2$	[a]	27.5
Cr_2O_3	1.4	24.8
1.7% $Mo(VI)/SiO_2$-aq	[a]	32.5
4.2% $Mo(VI)/SiO_2$-aq	[a]	30.2
8.4% $Mo(VI)/SiO_2$-aq	[a]	33.0
2.0% $Mo(VI)/SiO_2$-org	0.17	32.9
4.3% $Mo(VI)/SiO_2$-org	0.19	28.3
6.2% $Mo(VI)/SiO_2$-org	0.18	31.6
MoO_3	0.75	30.9

[a] TOFs cannot be accurately calculated for these samples due to the presence of crystallites (see Discussion).

DISCUSSION

For the $Cr(VI)/SiO_2$ catalysts, no crystallites can be seen by XRD up to a weight loading of 1.0% $Cr(VI)/SiO_2$ (Fig. 2)

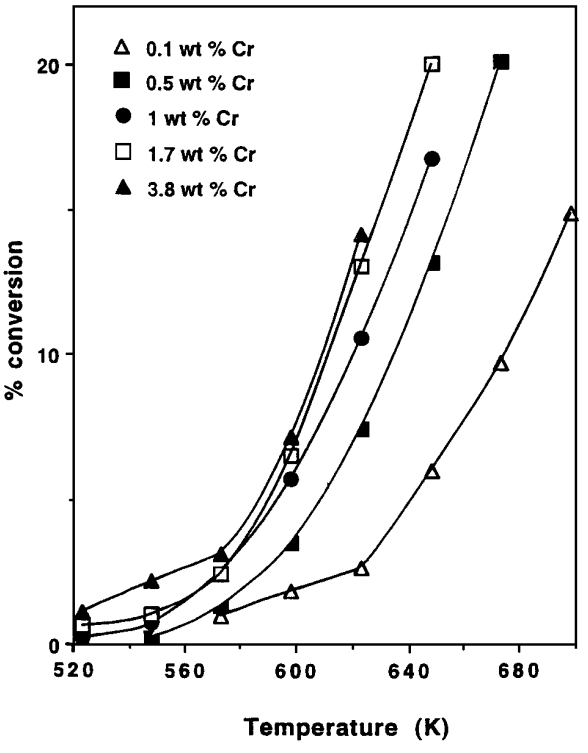

FIG. 12. Conversions over $Cr(VI)/SiO_2$ catalysts.

and the *in situ* Raman spectrum of the 1.0% $Cr(VI)/SiO_2$ catalyst shows that crystalline Cr_2O_3 is absent. The *in situ* 1.0% $Cr(VI)/SiO_2$ Raman spectrum is in excellent agreement with previous spectra published by Kim *et al.*, where the feature at 986 cm^{-1} is attributed to an isolated Cr species anchored to SiO_2 (40). Previous structural characterization work has established that Cr spreads on SiO_2, reacting with the hydroxyl groups, until all hydroxyl groups have reacted. This corresponds to about 2% Cr for a support like Cab-O-Sil HS 5 (40). The extensive literature on the Cr/SiO_2 system encompassing a variety of techniques like XPS, IR, TPO/TPR, UV-vis DRS and Raman (30, 31, 33–40), and our data convince us that the majority of the low weight loading Cr on SiO_2 is present as Cr(VI) when fully oxidized. While a small fraction could be present as Cr(III), no evidence for α-Cr_2O_3 is found. Also, we do not observe H_2, which is expected over Cr(III), as one of the products of 1-butene dehydrogenation. This further strengthens the assumption that the active centers on low weight loading $Cr(VI)/SiO_2$ catalysts are indeed Cr(VI) and not Cr(III). Thus, it is reasonable to assume that the 0.1, 0.5, and 1.0% $Cr(VI)/SiO_2$ catalysts used in this study contain completely dispersed Cr cations over SiO_2. Crystallites of Cr_2O_3 are clearly present for the 3.8% $Cr(VI)/SiO_2$ sample as seen by XRD (Fig. 2), and for this sample, both dispersed Cr cations and crystallites of Cr_2O_3 co-exist on the SiO_2 surface. Although Cr_2O_3 is not observed by XRD for the 1.7% $Cr(VI)/SiO_2$ sample, it is possible that very small crystallites are present since XRD is not a very sensitive technique if particle sizes are on the order of 1 nm. Unfortunately, Raman data could not be obtained for this sample due to fluorescence. Diffuse reflectance spectroscopy has been previously used to establish that the dispersed Cr cations over SiO_2 are in the 6+ oxidation state and the Cr cations in Cr_2O_3 crystallites are in the 3+ oxidation state (47).

In the case of the $Mo(VI)/SiO_2$ catalysts, the XRD patterns (Fig. 3) and the Raman spectra (Fig. 6) of the samples made via the organometallic route show no features attributable to crystalline MoO_3. The 993 cm^{-1} feature is a Mo=O stretch that has been assigned to an isolated Mo(VI) species (27, 29, 44). On the other hand, for the $Mo(VI)/SiO_2$ samples made via the aqueous route, the presence of MoO_3 crystallites is clearly observed by both XRD and Raman spectroscopy. These results are in complete agreement with previous work, where we have shown that control of the surface structure of Mo cations on SiO_2 is possible by choosing the appropriate preparation method (28, 29). For samples made via the aqueous route, although crystallites of MoO_3 are present, dispersed Mo species are also present (16, 29).

The Raman spectra (Fig. 7) of $W(VI)/SiO_2$ (Silice) and $W(VI)/SiO_2$ (Davison) show the W=O stretch of a dispersed W cation at 990 cm^{-1} as had been previously reported (30). Crystallites of WO_3 are evident from the 810 and 720 cm^{-1} features in the Raman spectra of the $W(VI)/SiO_2$ (Cab-O-Sil HS 5) sample (the same silica used for studying 1-butene oxidation). Dispersed W species and crystallites of WO_3 are assumed to coexist on the Cab-O-Sil HS 5 surface. Reasons for the dependence of dispersion on the SiO_2 support are not clear. One possible explanation is that the impurities present in Davison SiO_2 and Silice SiO_2 are responsible for stabilizing the W in a dispersed phase (Table 1). Only the $W(VI)/SiO_2$ samples made from Cab-O-Sil HS 5 were considered in the 1-butene oxidation study, as Cab-O-Sil HS 5 is relatively pure and relatively inert for 1-butene oxidation.

1,3-Butadiene formation activity increased with Mo weight loading (Fig. 9), indicating that Mo sites participate in the reaction, and at higher weight loadings more sites are available for reaction. A more important observation is that the TOF of bulk MoO_3 is three times higher than the TOFs for the fully dispersed $Mo(VI)/SiO_2$ catalysts (Table 2), suggesting there is a structure effect for 1-butene oxidation. Mo(VI) in crystalline MoO_3 is more active than dispersed Mo(VI). Some of the different crystalline planes present on MoO_3 could offer a favorable geometry to 1-butene adsorption and reaction, or could facilitate Mo(VI) reduction, when compared to the dispersed Mo(VI) species. Crystalline plane structure effects have been observed before by Kung and Kung for 1-butene oxidation over ferrite catalysts (11).

For the Mo(VI)/SiO_2 samples made via aqueous preparation methods, crystallites of MoO_3 coexist on the surface with some amount of dispersed Mo species. The exact ratio of dispersed Mo to the Mo present in crystallites could not be established. For the 8.4% Mo(VI)/SiO_2 sample, X-ray line broadening of the (110) and (021) peaks of MoO_3 allow us to estimate an approximate particle size of 18 nm. From the unit cell of the MoO_3 system, a rough calculation reveals that only 24% of the Mo atoms in a 18 nm MoO_3 crystallite are exposed. If all the Mo is assumed present as 18 nm crystallites, a TOF of 0.84×10^{-4} is obtained for this sample; the apparent TOF based on total Mo is 0.21×10^{-4}. This higher value agrees quite well with the TOF observed for bulk MoO_3 (Table 2). The correct TOF for the 8.4% Mo(VI)/SiO_2 sample will be between the two values, 0.21×10^{-4} and 0.84×10^{-4}, because not all the Mo is present in crystallites. We can only suggest that the number of surface Mo cations is less than the total number of Mo atoms. This implies that the real TOFs for the aqueous preparation samples are closer to that for bulk MoO_3 and reinforces the idea that there is a structure effect for 1-butene oxidation. Furthermore, the Mo results show caution must be exercised when basing TOF on total atoms present (16), or active sites established with titrations when dispersed and crystalline cations are present (13).

The activity of the Cr(VI)/SiO_2 catalysts increases with weight loading from 0.1 to 1.0%, and then is slightly lower for the 1.7 and 3.8% Cr(VI)/SiO_2 samples (Fig. 10). The TOFs for the 0.1, 0.5, and 1.0% Cr(VI)/SiO_2 catalysts, which were shown to be fully dispersed, are around 1.5×10^{-3}, an order of magnitude more active than bulk Cr_2O_3 (1.4×10^{-4}). The 1.7% sample is suspected of having Cr_2O_3 crystallites and the 3.8% sample was shown to have Cr_2O_3 crystallites; therefore TOFs cannot be calculated for these samples. It should be noted that the dispersed Cr cations in the Cr(VI)/SiO_2 catalysts are in the 6+ oxidation state, while the Cr cations in crystallites of Cr_2O_3 are in the 3+ oxidation state. Thus the differences in activity cannot be interpreted as a structural effect as in the case of the Mo(VI)/SiO_2 catalysts.

Our results indicate that the initial oxidation state and the subsequent red-ox nature of the cation plays a very important role for 1-butene oxidation. This argument is further strengthened when a comparison of the TOFs of dispersed Cr(VI) and dispersed Mo(VI) cations is made. Both these cations have similar structures and are in the same initial oxidation state of 6+. Table 2 shows that the dispersed Cr cations are at least one order of magnitude more active than the dispersed Mo cations.

The importance of cation red-ox nature in selective oxidation of 1-butene can be understood by examining the hydrogen abstraction steps. 1-Butene oxidation to 1,3-butadiene is a two-electron process. Homolytic or heterolytic hydrogen abstraction processes are possible and we cannot comment on the detailed pathway. The two-electron nature of the overall reaction reduces the cation from an oxidation state of n+ to (n − 2)+ (n = starting oxidation state; 6+ for dispersed Mo, W, and Cr; 6+ for Mo in MoO_3, 6+ for W in WO_3, and 3+ for Cr in Cr_2O_3). To regenerate the active site, reoxidation to the n+ oxidation state must take place.

The cation that most easily changes oxidation states is expected to be the most active. The cations studied here belong to group VIB of the periodic table, with differing red-ox abilities. Cr has the greatest ease of reduction from 6+ to 4+, the most stable oxidation state of Cr being 3+ (48). The presence of O_2 in the feed could facilitate reoxidation of the Cr cation from the 4+ to the 6+ oxidation state, thereby completing the cycle and regenerating the active site. In comparison, the reduction step is extremely difficult for the W cation, as it inherently prefers the 6+ oxidation state (48). The Mo cation is in between Cr and W in terms of its red-ox nature. Thus the activity in the selective oxidation of 1-butene follows the trend in red-ox ability, Cr > Mo > W. The Cr cation in bulk Cr_2O_3 is in the 3+ oxidation state, which is already the most stable oxidation state for Cr. It is much harder to reduce Cr(III) to facilitate the first step in hydrogen abstraction from the allylic carbon. This may explain why bulk Cr_2O_3 has a lower TOF than the dispersed Cr species. Thus ease of electron transfer is very important for the selective oxidation of 1-butene.

Similar arguments have been made in the case of ethanol oxidation over Mo(VI) catalysts supported on SiO_2, Al_2O_3, and TiO_2 by Zhang *et al.* (13). The reactivity sequence correlated with the molybdate–support interaction and the ease of reduction of surface molybdate. Wachs and co-workers have observed similar trends for supported V and Mo catalysts in methanol oxidation (14, 16). The differences in TOF for methanol oxidation by V cations over different supports were attributed to the nature of the M–O-support (M = Cr, Mo, or W) ligand and the red-ox ability of the catalysts. In addition, they found that, although the TOFs varied by a factor of 200, the activation energies were comparable. To account for the differences in the rates, the nature of the support was proposed to affect the preexponential factor of the apparent rate constant. Theoretical calculations by Weber for methanol oxidation have shown that the density of states or the availability of empty orbitals for electron transfer is a function of the support, with the more reducible supports like TiO_2 and ZrO_2 producing more active catalysts than refractory supports like SiO_2 and Al_2O_3. This was shown to affect the electronic partition function in the preexponential factor of the rate constant.

In our study, the only support used is SiO_2. But changing the supported cation (Cr, Mo, or W) is clearly seen to affect the activity of the catalysts, with the dispersed Cr(VI)/SiO_2 catalysts at least 50 times more active than the dispersed Mo(VI)/SiO_2 catalysts and the W(VI)/SiO_2 catalysts being inactive. The activation energies for all the 6+ catalysts are

comparable (Table 2). Structural characterization also established similar structures for fully dispersed Cr(VI) and Mo(VI) cations present over SiO_2. Differences in activity are therefore attributed to differences in the electronic partition function in the preexponential factor for the rate constant. More theoretical work is necessary before the origin of this effect can be understood properly.

CONCLUSIONS

The role of structure and the red-ox ability of the cation were investigated for the selective oxidation of 1-butene over $Cr(VI)/SiO_2$, $Mo(VI)/SiO_2$, and $W(VI)/SiO_2$ catalysts. For the $Mo(VI)/SiO_2$ system, a structure effect was observed with Mo(VI) in MoO_3 crystallites being three times more active than dispersed Mo(VI) for 1-butene selective oxidation. For the $Cr(VI)/SiO_2$ system, Cr in the 6+ oxidation state was 10 times more active than Cr in the 3+ oxidation state. Dispersed Cr(VI) is also 50 times more active for 1-butene selective oxidation than dispersed Mo(VI). The $W(VI)/SiO_2$ catalysts were not active for 1-butene oxidation. The differences in activity between Cr, Mo, and W cations in the 6+ oxidation state followed the trend in red-ox ability, where Cr > Mo > W. It is suggested that the origin of this cation red-ox effect could be associated with the electronic partition function associated with the preexponential factors of the rate constants for 1-butene oxidation.

ACKNOWLEDGMENTS

This work was supported by the U.S. Department of Energy, Office of Basic Energy Sciences under Grants DE-FG03-95ER14570 (University of Texas at Austin) and DE-FG02-93ER14350 (Lehigh University).

REFERENCES

1. Dadyburjor, D. B., Jewur, S. S., and Ruckenstein, E., *Catal. Rev. Sci. Eng.* **19**(2), 293 (1979).
2. Haber, J., *in* "New Developments in Selective Oxidation by Heterogeneous Catalysis" (B. Delmon, Ed.), Vol. 72, p. 279. Elsevier Science, Amsterdam, 1992.
3. Kung, H. H., *Ind. Eng. Chem. Prod. Res. Dev.* **25**, 171 (1986).
4. Centi, G., and Trifiro, F., *Appl. Catal.* **12**, 1 (1984).
5. Centi, G., *Catal. Lett.* **22**, 53 (1993).
6. Kung, H. H., "Transition Metal Oxides: Surface Chemistry and Catalysis," Studies in Surface Science and Catalysis, Vol. 45. Elsevier, New York, 1989.
7. Bond, G. C., Flamerz, S., and Shukri, R., *Farad. Discuss. Chem. Soc.* **87**, 65 (1989).
8. Wachs, I. E., Deo, G., Vuurman, M. A., Hu, H., Kim, D. S., and Jehng, J., *J. Molec. Catal.* **82**, 443 (1993).
9. Deo, G., Wachs, I. E., and Haber, J., *Crit. Iss. Surf. Chem.* (1994).
10. Kung, H. H., *ACS Symp. Ser.,* 545 (1983).
11. Kung, H. H., and Kung, M. C., *Adv. Catal.* **33**, 159 (1985).
12. Ono, T., Kamisuki, H., Hisashi, H., and Miyata, H., *J. Catal.* **116**, 303 (1989).
13. Zhang, W., Desikan, A., and Oyama, S. T., *J. Phys. Chem.* **99**, 14468 (1995).
14. Deo, G., and Wachs, I. E., *J. Catal.* **146**, 323 (1994).
15. Kim, D. S., and Wachs, I. E., *J. Catal.* **42**, 166 (1993).
16. Kim, D. S., Wachs, I. E., and Segawa, K., *J. Catal.* **146**, 268 (1994).
17. Tatibouet, J. M., Germain, J. E., and Volta, J. C. J., *J. Catal.* **82**, 240 (1983).
18. Iwasawa, Y., Nakano, Y., and Ogasawara, S., *J. Chem. Soc. Farad. Trans. I* **74**, 2986 (1978).
19. Ono, T., Nakagawa, Y., Miyata, H., and Kubokawa, Y., *Bull. Chem. Soc. Jpn* **57**, 1205 (1984).
20. Hu, H., and Wachs, I. E., *J. Phys. Chem.* **99**, 10911 (1995).
21. Desikan, A., Zhang, W., and Oyama, S. T., *J. Catal.* **157**, 740 (1995).
22. Weber, R. S., *J. Phys. Chem.* **98**, 2999 (1994).
23. Ramani, N. C., Sullivan, D. L., and Ekerdt, J. G., *J. Catal.* **173**(1), 105 (1998).
24. Escribano, V. S., Busca, G., and Lorenzelli, V., *J. Phys. Chem.* **95**, 5541 (1991).
25. Mori, K., Inomata, M., Miyamoto, A., and Murakami, Y., *J. Phys. Chem.* **87**, 4561 (1983).
26. Vuurman, M. A., Wachs, I. E., Stufkens, D. J., and Oskam, A. D., *J. Molec. Catal.* **80**, 209 (1993).
27. Hu, H., Wachs, I. E., and Bare, S. R., *J. Phys. Chem.* **99**, 10897 (1995).
28. Roark, R. D., Kohler, S. D., Ekerdt, J. G., Kim, D. S., and Wachs, I. E., *Catal. Lett.* **16**, 231 (1992).
29. Williams, C. C., Ekerdt, J. G., Jehng, J-M., Hardcastle, F. D., Turek, A. M., and Wachs, I. E., *J. Phys. Chem.* **95**, 8781 (1991).
30. Kim, D. S., Ostromecki, M., Wachs, I. E., Kohler, S. D., and Ekerdt, J. G., *Catal. Lett.* **33**, 209 (1995).
31. Kim, D. S., Ostromecki, M., and Wachs, I. E., *J. Mol. Catal. A: Chemical* **106**, 93 (1996).
32. Roark, R. D., Kohler, S. D., and Ekerdt, J. G., *Catal. Lett.* **16**, 77 (1992).
33. Weckhuysen, B. M., and Wachs, I. E., *J. Phys. Chem.* **100**, 14437 (1996).
34. Merryfield, R., McDaniel, M. P., and Parks, G., *J. Catal.* **77**, 348 (1982).
35. Kim, C. S., and Woo, S. I., *J. Molec. Catal.* **73**, 249 (1992).
36. McDaniel, M. P., *J. Catal.* **76**, 17 (1982).
37. McDaniel, M. P., *J. Catal.* **76**, 37 (1982).
38. Zecchina, A., Garrone, E., Ghioti, G., Morterra, C., and Borello, E., *J. Phys. Chem.* **79**, 966 (1975).
39. Weckhuysen, B. M., De Ridder, L. M., and Schoonheydt, R. A., *J. Phys. Chem.* **97**, 4756 (1993).
40. Kim, D. S., Tatibouet, J., and Wachs, I. E., *J. Catal.* **136**, 209 (1992).
41. Sullivan, D. L., Roark, R. D., Ekerdt, J. G., Deutsch, S. E., and Gates, B. C., *J. Phys. Chem.* **99**, 3678 (1995).
42. Roark, R. D., Narayanan, C. R., Sullivan, D. L., and Ekerdt, J. G., *Chem. Mater.* **6**, 739 (1994).
43. Hardcastle, F. D., and Wachs, I. E., *J. Molec. Catal.* **46**, 173 (1988).
44. Banares, M. A., Hu, H., and Wachs, I. E., *J. Catal.* **150**, 407 (1994).
45. Ziolkowski, J., *J. Catal.* **80**, 263 (1983).
46. JCPDS Powder Diffraction File, Pattern 38 : 1479.
47. Bensalem, A., Weckhuysen, B. M., and Schoonheydt, R. A., *J. Phys. Chem. B* **101**, 2824 (1997).
48. Weast, R. W. (Ed.), "CRC Handbook of Chemistry and Physics," 61st, ed., CRC Press, Boca Raton, FL, 1981.